An Efficient High-Step-Up Soft-Switching Boost Converter for Photovoltaic Application

Mahdi Akhbari
Assistant Professor
akhbari@shahed.ac.ir

Pouya Amiri
M.Sc. Student
amiri.pouya@gmail.com

Mohamad S. Nilsaz
M.Sc. Student
nilsaz.mohamad@gmail.com

Electrical and Electronic Engineering Department, Shahed University,
Tehran, Iran, Email: akhbari@shahed.ac.ir

***Abstract*—In this paper, an efficient high step-up boost converter with a coupled-inductor with soft-switching operation is presented. The proposed topology includes a coupled-inductor boost converter for raising the voltage gain. Moreover, a simple auxiliary resonant circuit composed of an auxiliary switch, a clamping diode and a resonant tank (inductor, capacitor), is adopted in this paper. The coupled-inductor boost converter presents poor efficiency because of hard switching and switch losses. All switches in the adopted circuit perform zero-current switching at turn-on, and zero-voltage switching at turn-off. This soft-switching operation reduces the switching losses and diode reverse-recovery problems. The converter uses PWM method for switching and it is controlled by a PI controller to improve its dynamic response. The paper presents detailed analysis of the converter operational modes. A 225W dc-dc converter is designed and evaluated by simulations. The results are presented to confirm the theoretical analysis.**

***Keywords*—Boost converter, High-step-up Converter, Coupled-inductor, Soft-switching.**

I. INTRODUCTION

High step-up dc-dc converters have many industrial applications such as uninterruptible power supplies (UPS), telecommunications industry, space industry, distributed energy generating systems using renewable energy sources and hybrid electric vehicles (HEV). These applications use low voltage energy sources such as batteries, ultra-capacitors, fuel cells and PV cells and require much higher output voltage for operation. In theory, conventional boost converters are able to provide high voltage gain with an extreme duty cycle. However, in practice, the voltage gain is limited by parasitic resistance of boost inductor and switching devices, and instability at high operating duty cycles because of diode reverse-recovery. There also higher voltage devices are necessary and it results in cost increase and lower efficiency. To increase both voltage gain and conversion efficiency, many modified boost converters have been developed in recent years [1]–[4].

To overcome the diode reverse-recovery problems, active-clamp techniques were adopted but voltage gain and efficiency were still limited by turn-on time and loss of the auxiliary switch losses respectively.

To achieve a wide voltage ratio and decrease both voltage and current stresses and reverse-recovery problems coupled-inductor were employed but the leakage energy of coupled-inductor resulted in high voltage stress across the switch at turn-off. To protect the switches, either a high-rated switch or a snubber circuit was needed. To consume the leakage energy and moderate voltage stress and output diode peak voltage passive snubber circuits were implemented [2]–[4].

Another problem is switching losses, which is problematic especially at high switching frequencies which results in poor converter efficiency. Therefore, to reduce these switching losses soft-switching methods were applied [5]. Also a soft-switching method is proposed, which involves an auxiliary circuit. However, the auxiliary resonant circuit increases the cost and complexity of converter [6]–[16]. In certain cases in the resonant converters formed by an auxiliary switch, the main switch achieves soft-switching but the auxiliary switch performs hard-switching. Thus, the whole system efficiency remains relatively poor owing switching losses of the auxiliary switch. Park *et al.* [17] presented a soft-switching boost converter applied to an auxiliary resonant circuit. They obtained better efficiency comparing conventional boost converter. The adopted converter has a simple auxiliary resonant circuit (SARC). Through this circuit, all of the switching devices perform soft-switching under zero-voltage and zero-current conditions. Therefore, the periodic switching losses generated at switches turn-on and turn-off can be decreased. However, the proposed converter has low dc voltage conversion ratio due to none ideal circuit components.

This paper proposes a new converter topology that presents the both high voltage conversion ratio and efficiency. As illustrated in Fig. 1, the converter is an adopted coupled-inductor boost dc-dc converter using a resonant circuit. In the proposed converter all switching devices perform soft-switching under ZVS and ZCS reducing the losses and voltage and current stresses. The converter uses PWM method for switching patterns and is controlled by a PI controller to improve its dynamic output response. A 225W dc-dc converter for PV application is designed and evaluated by simulation in PSIM software. The results show a good agreement with analytical findings. Before mounting the prototype, the design parameters of the converter should be optimized to minimize the losses and to limit switching

stresses, now the research activities are in progress to achieve this aim.

II. CONVERTER ANALYSES AND DESIGN

In Fig. 1, the adopted converter is including three parts, a coupled-inductor boost converter, auxiliary resonant circuit and clamp diode (D_c). Shown in Fig. 2, the operational mode of this converter can be divided into six modes. For a simple analysis of each mode, the following assumptions are made:

1) All switching devices and passive elements are ideal.
2) The converter operates in continuous conduction mode at all modes.
3) The input voltage (V_s) is considered constant.
4) The coupled inductor in Fig. 1 is modeled as a transformer with magnetizing inductor (L_m) as depicted in Fig. 2. The turns ratio (n) and coupling coefficient (k) of the transformer are defined by the relations (1) and (2) where N_1 and N_2 are the winding turns in the primary and secondary sides, respectively.

$$n = N_2/N_1 \quad (1)$$

$$k = L_m/(L_m + L_l) \quad (2)$$

The voltage gain of coupled-inductor boost converter and the voltage stress on the main switches ($V_{s1,2}$) are calculated as (3) and (4), where D is the duty cycle of the switches. These relationships are derived from the analysis of the proposed converter which is presented by 6 modes of operation during a switching period in the next sub-sections.

$$V_o/V_s = (nD + 1)/(1 - D) \quad (3)$$

$$v_{S1,S2} = (nv_s + v_o)/(n + 1) \quad (4)$$

Mode 1 ($t_0 \le t < t_1$)

Switches S_1 and S_2 are both in the OFF state, the current cannot flow through switches S_1andS_2, and the accumulated energy of the L_m is transferred to the load (Fig. 3). In this mode, the L_m current decreases linearly. During this time, the current does not flow to the resonant inductor (L_r), and the resonant capacitor (C_r) is charged by a constant amount. After both switches are turned on, mode 1 is over; the relations describing some of the voltages and the currents may be simply obtained as follows:

$$v_{Lm}(t) = (V_s - V_o)/(n + 1) \quad (5)$$

$$i_{Lm}(t) = i_{Lm}(t_0) + \frac{(V_s - V_o)}{(n+1)L_m}t \quad (6)$$

$$i_{Do}(t) = i_{Lm}(t)/n \quad (7)$$

$$i_{Lr}(t) = i_{s1,s2}(t) = i_{D1,D2}(t) = 0 \quad (8)$$

$$v_{cr}(t) = (nv_s + v_o)/(n + 1) \quad (9)$$

$$v_{S1,S2} = v_{cr}(t)/2 \quad (10)$$

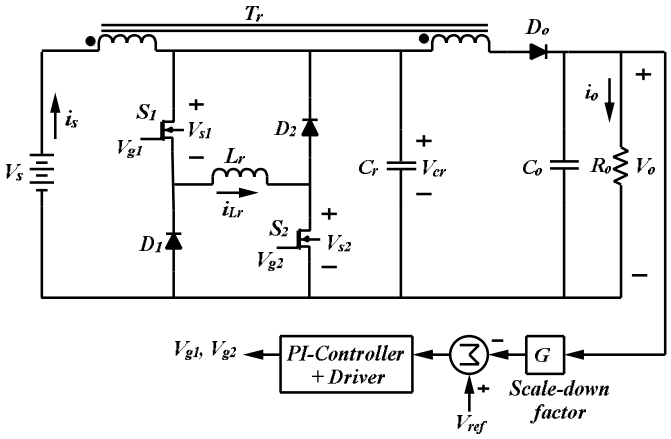

Fig.1 Topology of the proposed converter

Mode 2 ($t_1 \le t < t_2$)

After turning on the switches S_1 and S_2, the current flows to the resonant inductor. At that time, the both switches are turned on under zero-current switching (ZCS). As the resonant current rises linearly, the load current gradually decreases. The resonant capacitor voltage will be constant. Att_2, the magnetizing inductor current equals the resonant inductor current, and the output diode (D_o) current reaches zero. Then, the output diode is turned off under zero-current switching (ZVS), and mode 2 is over:

$$i_{Lr}(t_1) = 0 \quad , \quad v_{Lr}(t) = v_{cr}(t) \quad (11)$$

$$i_{Lr}(t) = i_{s1,s2}(t) = \frac{v_{cr}(t)}{L_r}t \quad (12)$$

$$i_{Lm}(t) = i_{Lm}(t_1) + \frac{(V_s - V_o)}{(n+1)L_m}t \quad (13)$$

$$i_{Lm}(t_2) = i_{Lr}(t_2) \quad (14)$$

$$i_{Do}(t) = i_{Lm}(t)/n \ , \ i_{Do}(t_2) = 0, i_{D1,D2}(t) = 0 \quad (15)$$

Mode 3 ($t_2 \le t < t_3$)

The output diode (D_o) current no longer flows, and the resonant capacitor (C_r) and the resonant inductor (L_r) start a resonance. The magnetizing inductor current is nearly constant. Hence, the magnetizing inductor voltage is near zero:

$$i_{Lm}(t) \cong I_{min} \quad , \quad v_{Lm} \cong 0 \quad (16)$$

$$i_{Lr}(t) = i_{s1,s2}(t) = I_{min} + \frac{V_M}{Zr}\sin(\omega_r t), i_{Lr}(t_3) = I_M \quad (17)$$

During this resonant period, the resonant capacitor is discharged from $(nv_s + v_o)/(n + 1)$ to zero. This is expressed as (18) and (19). Resonant frequency and impedance are given by (20). When the voltage of the resonant capacitor equals zero, the mode 3 is over:

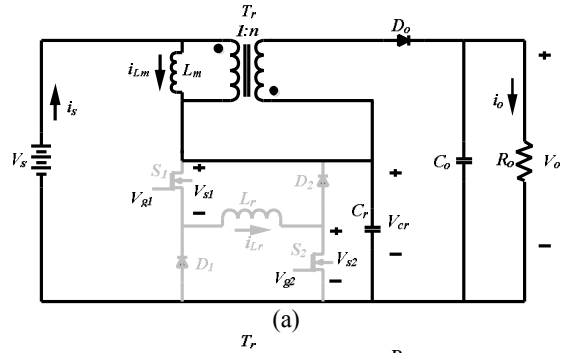

(a)

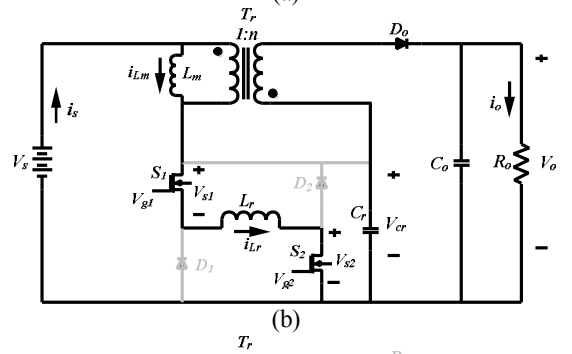

(b)

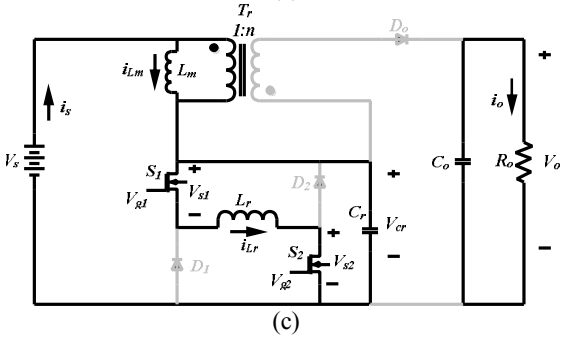

(c)

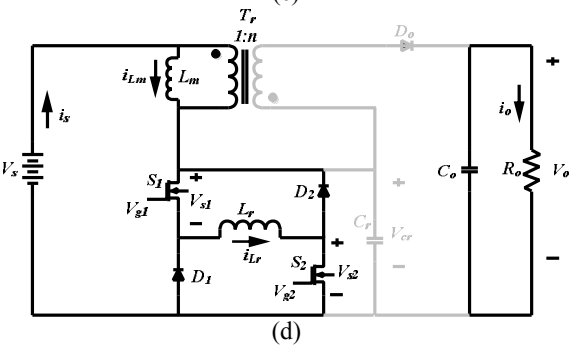

(d)

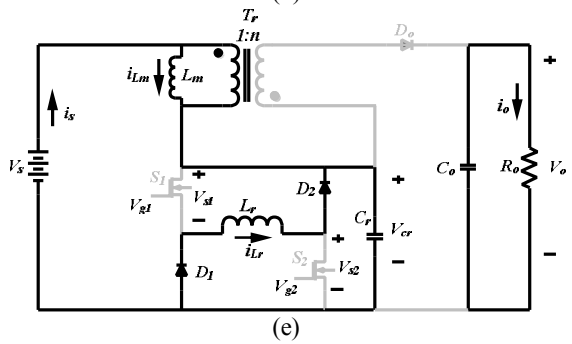

(e)

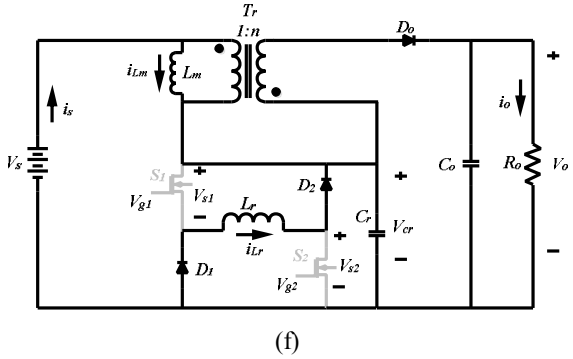

(f)

Fig.2 Operational modes of the proposed converter

a) Mode 1 b) Mode 2 c) Mode 3 d) Mode 4 e) Mode 5 f) Mode 6

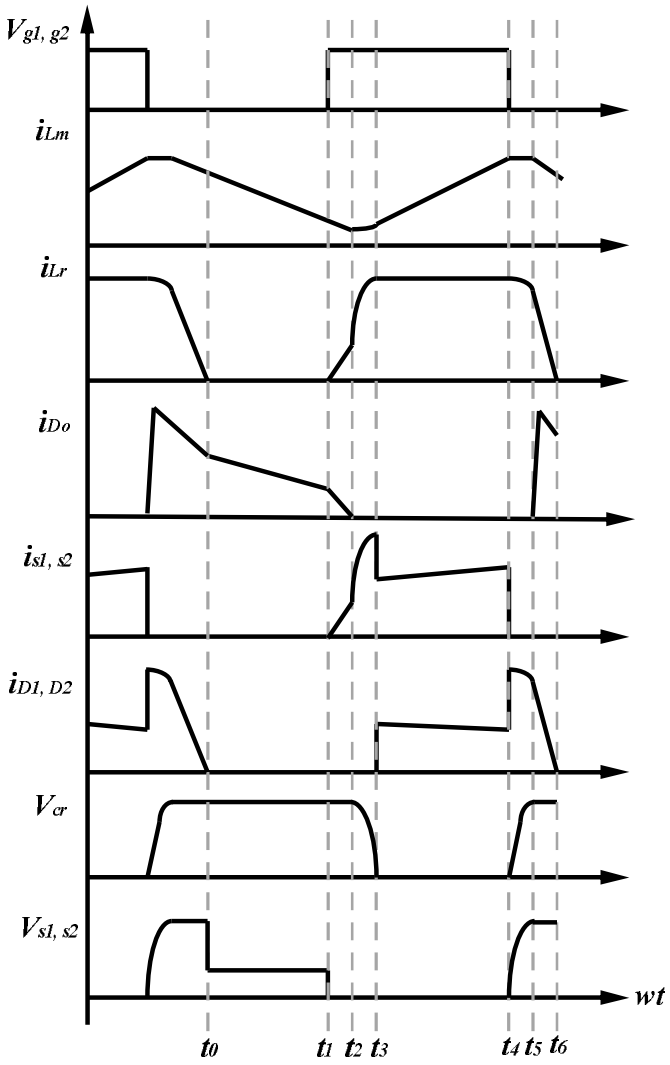

Fig.3 Waveforms according to operational modes analysis

$$v_{Cr}(t) = V_M \cos(\omega_r t) \quad (18)$$

$$v_{Cr}(t_2) = V_M = (nv_s + v_o)/(n+1),\ v_{Cr}(t_3) = 0 \quad (19)$$

$$\omega_r = 1/\sqrt{L_r C_r} \quad , \quad Z_r = \sqrt{L_r/C_r} \tag{20}$$

$$\mathrm{i_{Do}(t) = i_{D1,D2}(t) = V_{s1,s2}(t) = 0} \tag{21}$$

Mode 4 ($t_3 \le t < t_4$)

When the voltage of the resonant capacitor equals zero, mode 4 begins. In this mode, the freewheeling diodes of D_1 and D_2 are turned on, and the current of the resonant inductor is at maximum value. The resonant inductor current flows to the freewheeling paths S_1–L_r–D_2 and S_2–L_r–D_1:

$$i_{s1,s2}(t) = (i_{Lr}(t)/2) + (i_{Lm}(t)/2) \tag{22}$$

$$i_{D1,D2}(t) = (i_{Lr}(t)/2) - (i_{Lm}(t)/2) \tag{23}$$

$$i_{Lr}(t_3) = i_{Lr}(t_4) = I_{Lr,max} \tag{24}$$

During this time, the magnetizing inductor voltage is equal the input voltage and the current accumulating energy increases linearly:

$$v_{Lm}(t) = V_s \tag{25}$$

$$i_{Lm}(t) = I_{min} + \frac{V_s}{L_m} t \tag{26}$$

$$i_{Do}(t) = V_{cr}(t) = 0 \tag{27}$$

Mode 5 ($t_4 \le t < t_5$)

In mode 5, all of switches are turned off under the zero-voltage condition by the resonant capacitor. When all of the switches are turned off, the resonant capacitor C_r is charged to a constant value by the two inductor currents until the resonant capacitor is full charged and the output diode is in the OFF state.

$$i_{Lm}(t) \cong i_{Lm}(t4) = I_{max} \tag{28}$$

$$i_{Lr} = i_{D1,D2}(t) = I_{max}\cos(\omega_r t) \tag{29}$$

$$v_{Cr}(t) = v_{S1,S2}(t) = Z_r(I_{Lm}(t) + I_{Lr}(t))\sin(\omega_r t) \tag{30}$$

$$v_{Cr}(t_5) = (nv_s + v_o)/(n+1) \tag{31}$$

$$i_{Do}(t) = i_{s1,s2}(t) = 0 \tag{32}$$

Mode 6 ($t_5 \le t < t_6$)

When the resonant capacitor voltage equals a constant value mode 6 begins. The output diode is turned on under the zero-voltage condition. During this mode, the magnetizing inductor current i_{Lm} and the resonant inductor current i_{Lr} flow to the output through the output diodeD_o:

$$i_{Do}(t) = (i_{Lm}(t)/n) + i_{Lr}(t) \tag{33}$$

$$i_{Lr}(t) = \left(-\frac{v_{Cr}(t)}{L_r}\right)t \,,\; i_{Lr}(t_6) = 0 \tag{34}$$

$$v_{Cr}(t) = (nv_s + v_o)/(n+1) \tag{35}$$

$$v_{S1,S2}(t) = v_{Cr}(t) \tag{36}$$

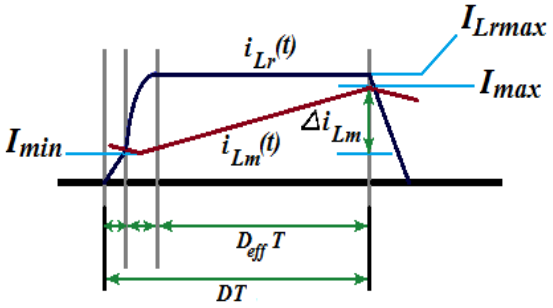

Fig.4 ZVS condition

Both inductor currents are linearly decreased, and the energy of the resonant inductor is completely transferred to the load. Then, the mode 6 is over:

$$i_{Lm}(t) = I_{max} + \frac{(V_s - V_o)}{(n+1)L_m} t \tag{37}$$

III. DESIGN PROCEDURE

A. ZVS Condition of Switch

Fig. 4 shows the key waveform of the soft-switching converter. The minimum and maximum values of the duty cycle are obtained from magnetizing inductor voltage as (38) and (39) respectively. The resonant inductor current must exceed the magnetizing inductor current during the freewheeling mode (mode 4) to satisfy the zero-voltage switching (ZVS) condition. The voltage of the resonant inductor and the current are expressed as (40) and (41), respectively.

$$D_{min} = \frac{V_o - V_{S,max}}{(nV_{s,max} + V_o)} \tag{38}$$

$$D_{max} = \frac{V_o - V_{S,min}}{(nV_{s,min} + V_o)} \tag{39}$$

$$v_{Lr}(t) = -(V_{s1} + V_F) = -V_{FW} \tag{40}$$

$$i_{Lr}(t) = -\frac{V_{FW}}{L_r} t + I_{min} + \frac{(nV_s + V_o)}{(n+1)Z_r} \tag{41}$$

The ZVS condition of this converter is expressed as (42)

$$-\frac{V_{FW}}{L_r} t + I_{min} + \frac{(nV_{s,min} + V_o)}{(n+1)Z_r} > I_{max} \tag{42}$$

$$I_{max} = I_{min} + \Delta i_{Lm} \tag{43}$$

$$-\frac{V_{FW}}{L_r} D_{max} T + \frac{(nV_{s,min} + V_o)}{(n+1)Z_r} > \Delta i_{Lm} \tag{44}$$

B. Resonant Inductor

In Fig. 4, the rising time of the resonant inductor current (mode 2), is expressed by (45). For the maximum resonant current, the resonant time of the resonant inductor and capacitor (mode 3), is defined as one-fourth of the resonant period. As a rule of thumb, the rising time of the resonant inductor current (modes 2–3) can be set to 10% of the minimum on time. This is expressed by the relation (47):

$$t_3 - t_2 = \frac{L_r(n+1)}{nV_{s,min}+V_o} I_{min} \quad (45)$$

$$t_3 - t_1 = T_r/4 \quad (46)$$

$$\frac{L_r(n+1)}{nV_{s,min}+V_o} I_{min} + \frac{T_r}{4} = 0.1 D_{min} T \quad (47)$$

From (44) and (47), the resonant inductor is determined by:

$$L_r < \frac{\left[\frac{0.2(nV_{s,min}+V_o)}{\pi(n+1)} D_{min} T - V_{FW} D_{max} T\right]}{\left[\Delta i_{Lm} + \frac{2}{\pi} I_{min}\right]} \quad (48)$$

C. Resonant Capacitor

The resonant capacitor is connected to the switches in parallel. Thus, the waveforms of the resonant capacitor voltage and switch voltage are equivalent at turn-off (modes 5 and 6). The resonant capacitor can be selected to exceed ten times the output capacitance of the switch to satisfy the ZVS condition. Since the capacitor is charged by the magnetizing inductor current and the resonant inductor current during mode 5, it can be selected to exceed twenty times the output capacitance of the switch. Equation (47) is simplified to:

$$C_r = \frac{0.04 D_{min}^2 T^2}{\pi^2 L_r} + \frac{4\left(\frac{(n+1)}{nV_{s,min}+V_o}\right)^2 L_r I_{min}^2}{\pi^2} - \frac{0.8\frac{(n+1)}{nV_{s,min}+V_o} D_{min} T I_{min}}{\pi^2} \quad (49)$$

The above mentioned relationships are used to determine the main parameters of a 225W power converter considered for photovoltaic application. Table. I gives the converter specifications and parameters.

The design of the resonant inductor and capacitor are based on relations (48) and (49). More investigations are being performed to determine an optimized design of the converter by taking in to account the switching losses and stresses.

To have a comparison between the proposed soft-switching converter and hard-switching converter losses, the loss analyses have been carried out. The main losses include the turn-on and turn-off switching losses, the switching losses due to the drain-source capacitance of MOSFETs and the junction capacitance of diodes. The loss equations can be obtained through the loss analysis of each stage (see [18]). The ratio of the proposed soft-switching converter losses (P_{Soft}) over the hard-switching converter losses (P_{Hard}) have been plotted in Fig. 5. From this figure, it can be seen that at the same turn ratio, the loss ratio rises by increase of voltage gain. It is because to reach a higher voltage gain at a constant turn ratio, duty cycle has to rise (3) and the ZVS condition of switching always comes at the expense of increase in conduction losses due to the use of extra diodes or auxiliary switches. For the worst condition ($V_s = 18V$) and the best condition ($V_s = 24V$) the soft-switching converter losses are about 68% and 61% of the hard-switching converter losses respectively.

TABLE I. CONVERTER SPECIFICATIONS AND IMPLEMENTATION DETAILS

Maximum Power	P_o	225[W]
Switching Frequency	f_s	100[KHz]
Input Voltage	V_s	18-24[V]
Output Voltage	V_o	150[V]
Magnetizing Inductor	L_m	200 [μH]
Resonant Inductor	L_r	0.5 [μH]
Resonant Capacitor	C_r	360 [nF]
Output Capacitor	C_o	100[μF]
Turns Ratio	n	6

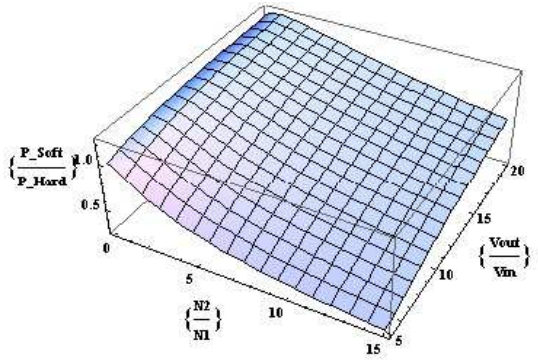

Fig.5 Loss comparison between proposed soft-switching converter (P_{Soft}) and hard-switching converter (P_{Hard})

I. SIMULATION RESULTS

The designed converter is simulated by using the PSIM software. In simulations all circuit elements are considered ideal. The converter specifications and implementation details are shown in Table I.

Fig. 6 shows the output diode current and switches current $S_{1,2}$. In this figure the ZVS and ZCS of the main switches and the output diode can be observed.

Fig. 7 shows the resonant capacitor voltage and drain-to-source voltage of the switches. As shown in this figure the voltage stress on the switches is clamped to resonant capacitor voltage. Via resonance of the resonant inductor and capacitor, ZVS and ZCS switching are achieved at turn-on and turn-off.

Fig. 8 shows the simulated waveforms of the magnetizing inductor current and the resonant inductor current. Since the resonant inductor current exceeds the magnetizing inductor current ZVS for switch is satisfied.

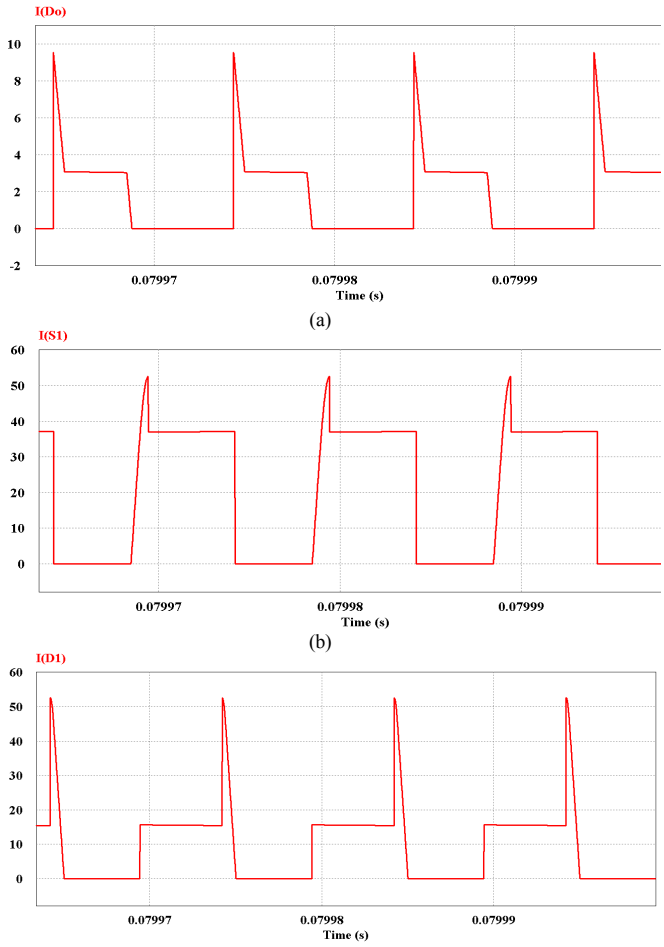

Fig.6 (a) Output diode current (b) switches current and (c) diodes current D_1 and D_2

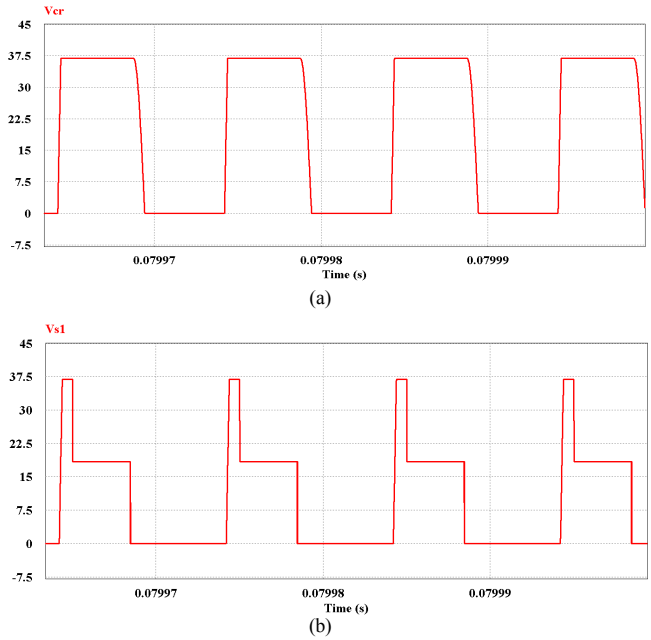

Fig.7 (a) Resonant capacitor voltage (b) switches voltage

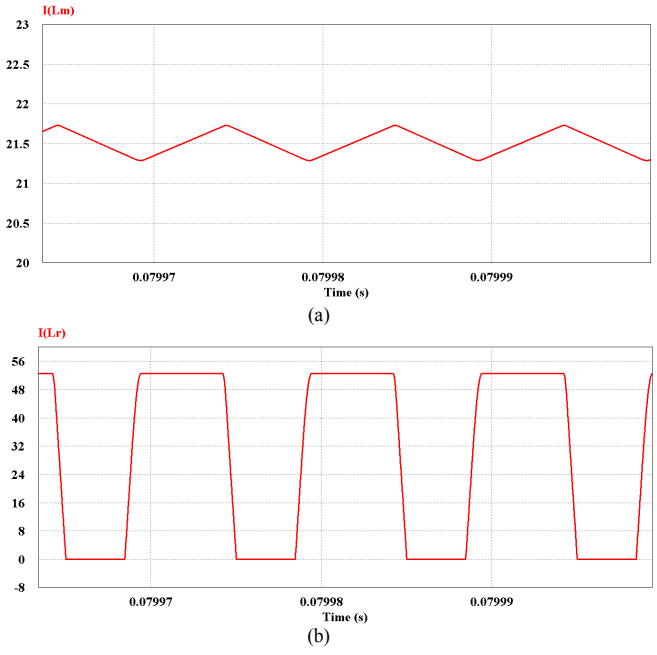

Fig.8 (a) Magnetizing inductor current (b) resonant inductor current

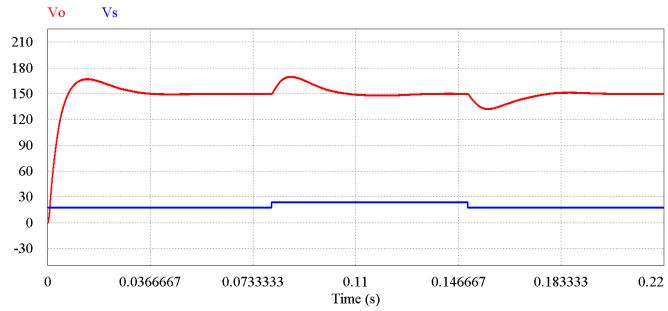

Fig.9 Dynamic response of the output voltage to a 30% source voltage changes

The input voltage is considered 18-24V to show the variant input voltage of the PV module as source. The maximum duty cycle for PWM is 0.51 and it can be raised to achieve higher voltage ratio.

Fig. 9 shows the dynamic response of the output voltage to the source voltage changes. At first, source voltage changes from 18V to 24V and then returns to 18V. As can be seen in this figure a time response of 20msec is obtained with a PI controller in which the coeffitients are ajusted by try and error.

II. CUNCLUSION

An efficient high step-up coupled-inductor soft-switched boost converter is developed in this paper. In the proposed converter all switching devices including main and auxiliary switches and output diode are working under ZVS and ZCS in torn-off and turn-on. Therefore, the switching losses are reduced dramatically and the output diode reverse-recovery problem has no longer existed. Also due to resonant circuit, the voltage stress is limited to an acceptable value. Operational modes of the converter are specified and analyzed, then, the main relationships of the converter are

determined from this analysis. A design procedure is suggested based on the main relationships of the converter. A 225W dc-dc converter is designed and simulated. The simulation results show a good agreement with analytical approach in both operational modes and waveform characteristics.

REFERENCES

[1]. Emadi, K. Rajashekara, S. S. Williamson, and S. M. Lukic, "Topological overview of hybrid electric and fuel cell vehicular power system architectures and configurations," *IEEE Trans. Veh. Technol.*, vol. 54, no. 3, pp. 763–770, May 2007.

[2]. Q. Zhao and F. C. Lee, "High-efficiency, high step-up dc–dc converters," IEEE Trans. Power Electron., vol. 18, no. 1, pp. 65–73, Jan. 2003.

[3]. J. Bauman and M. Kazerani, "A comparative study of fuel cell-battery, fuel cell-ultracapacitor, and fuel cell-battery-ultracapacitor vehicles," IEEE Trans. Veh. Technol., vol. 57, no. 2, pp. 760–769, Mar. 2008.

[4]. W. Rong-Jong and D. Rou-Yong, "High Step-Up Converter With Coupled-Inductor," IEEE Trans. Power Electron., vol. 20, no. 5, Sep. 2005.

[5]. S. da Silva, L. dos Reis Barbosa, J. B. Vieira, L. C. de Freitas, and V. J. Farias, "An improved boost PWM soft-single-switched converter with low voltage and current stresses," IEEE Trans. Ind. Electron., vol. 48, no. 6, pp. 1174–1179, Dec. 2001.

[6]. H. Bodur and A. Faruk Bakan, "A new ZCT-ZVT-PWM DC–DC converter," IEEE Trans. Power Electron., vol. 19, no. 3, pp. 676–684, May 2004.

[7]. S. Zheng and D. Czarkowski, "Modeling and digital control of a phase controlled series parallel resonant converter," IEEE Trans. Ind. Electron., vol. 54, no. 2, pp. 707–715, Apr. 2007.

[8]. M. Z. Youssef and P. K. Jain, "Series parallel resonant converter in self-sustained oscillation mode with the high frequency transformer leakage inductance effect: Analysis, modeling, and design," IEEE Trans. Ind. Electron., vol. 54, no. 3, pp. 1329–1341, Jun. 2007.

[9]. R. Casanueva, F. J. Azcondo, and C. Branas, "Output current sensitivity analysis of the LCpCs resonant inverter: Current source design criteria," IEEE Trans. Ind. Electron., vol. 54, no. 3, pp. 1560–1568, Jun. 2007.

[10]. J. Tschirhart and P. K. Jain, "A CLL resonant asymmetrical pulse width modulated converter with improved efficiency," IEEE Trans. Ind. Electron., vol. 55, no. 1, pp. 114–122, Jan. 2008.

[11]. S.-S. Lee and G.-W. Moon, "Full ZVS range transient current buildup half bridge converter with different ZVS operations to load variation," IEEE Trans. Ind. Electron., vol. 55, no. 6, pp. 2557–2559, Jun. 2008.

[12]. X. Wu, J. Zhang, X. Ye, and Z. Qian, "Analysis and derivations for a family ZVS converter based on a new active clamp ZVS cell," IEEE Trans. Ind. Electron., vol. 55, no. 2, pp. 773–781, Feb. 2008.

[13]. J.-J. Lee, J.-M. Kwon, E.-H. Kim, and B.-H. Kwon, "Dual series resonant active clamp converter," IEEE Trans. Ind. Electron., vol. 55, no. 2, pp. 699–710, Feb. 2008.

[14]. J.-H. Kim, D.-Y. Yung, S.-H. Park, C.-Y.Won, Y.-C. Jung, and S.-W. Lee, "High efficiency soft-switching boost converter using a single switch," J. Power Electron., vol. 9, no. 6, pp. 929–939, Nov. 2009.

[15]. J.-P. Lee, B.-D. Min, T.-J. Kim, D.-W. Yoo, and J.-Y. Yoo, "Design and control of novel topology for photovoltaic dc/dc converter with high efficiency under wide load ranges," J. Power Electron., vol. 9, no. 2, pp. 300–307, Mar. 2009.

[16]. Shelas Sathyan, H. M. Suryawanshi, M. S. Ballal and A. B. Shitole, "Soft Switching DC-DC Converter for Distributed Energy Sources With High Step Up Voltage Capability", IEEE Trans. Ind. Electron., vol. 62, No. 11, July 2015.

[17]. S.-H. Park, Gil-Ro Cha, Yong-Chae Jung, and Chung-Yuen Won, "Design and Application for PV Generation System Using a Soft-Switching Boost Converter With SARC," IEEE Trans. Ind. Electron. vol. 57, no. 2, Feb. 2010.

[18]. Jun-Young Lee, Yu-Seok Jeong, and Byung-Moon Han, "An Isolated DC/DC Converter Using High-Frequency Unregulated LLC Resonant Converter for Fuel Cell Applications", IEEE Trans. Ind. Electron., vol. 58, No. 7, July 2011.